NJC

Accepted Manuscript

This is an *Accepted Manuscript*, which has been through the Royal Society of Chemistry peer review process and has been accepted for publication.

Accepted Manuscripts are published online shortly after acceptance, before technical editing, formatting and proof reading. Using this free service, authors can make their results available to the community, in citable form, before we publish the edited article. We will replace this *Accepted Manuscript* with the edited and formatted *Advance Article* as soon as it is available.

You can find more information about *Accepted Manuscripts* in the Information for Authors.

Please note that technical editing may introduce minor changes to the text and/or graphics, which may alter content. The journal's standard Terms & Conditions and the Ethical guidelines still apply. In no event shall the Royal Society of Chemistry be held responsible for any errors or omissions in this *Accepted Manuscript* or any consequences arising from the use of any information it contains.

ROYAL SOCIETY OF CHEMISTRY

www.rsc.org/njc

Journal Name

RSCPublishing

ARTICLE

Hybrid polymer thin films with lanthanide-zeolite A host-guest system: coordination bonding assembly and photo-integration

Cite this: DOI: 10.1039/x0xx00000x

Received 00th January 2012,
Accepted 00th January 2012

DOI: 10.1039/x0xx00000x

www.rsc.org/

Ji-Na Hao, Bing Yan*

A series of novel polymer-lanthanide-zeolite A have been synthesized by polymerization of ethyl methacrylate (EMA) and 4-vinylpyridine (4VP) containing surface modified zeolite A, inside the channels of which lanthanide complexes are incorporated. The surface modification was conducted by first functionalizing zeolite A with a multi-functional linker and then covalently grafting lanthanide ions which coordinates to both the molecular linker and the polymer chain. SEM images suggest that lanthanide-based zeolite A particles are evenly dispersed in the polymer matrices, leading to a certain transparency of the thin films. The luminescence properties of the resulting materials were characterized in detail and the results reveal that all the materials exhibit intense emission lines upon UV-light irradiation. Various emitting colors of the zeolite A-polymer materials can be obtained by simply changing the lanthanide complexes inside and outside the channels of zeolite A. Furthermore, the white light-emitting from the tricolor luminous materials can be easily obtained by adjusting the different concentration of the doped ions and the excitation wavelength.

Introduction

Numerous photoluminescent lanthanide-containing organic/inorganic hybrid materials have been developed considerably in the past few years for their excellent optical properties and the specific functions to be widely applied in various fields such as fluorescent biology, fluoroimmunoassays,[1] NIR-emitting probes and amplifiers for optical communications.[2] These kinds of materials have the capability of exploiting the synergy between the intrinsic characteristics of organic–inorganic hybrid hosts (mechanical, optical and/or electronic properties, thermal and chemical stability, highly controlled purity, versatile shaping and patterning, easy control of the refractive index, photosensitivity, encapsulation of large amounts of isolated emitting centers, biocompatibility and hydrophobic-hydrophilic balance) and the luminescence features of lanthanide complexes (high luminescence quantum yield, narrow bandwidth, long-lived emission, large stokes shifts, and ligand-dependent luminescence sensitization).[3] The nature of the interaction between the organic and inorganic components or phases has been used to classify such hybrid materials into two different classes.[4] Class I is the so-called physical doped hybrids in which there are no covalent or ion-covalent bonds between the organic and inorganic components. In such materials, there only exist week interactions such as hydrogen bonding, van der Waals forces, or weak static effects.[5] Class II is the chemically bonded hybrids in which the organic and inorganic counterparts are linked through strong interactions such as covalent, ion-covalent, coordination, or Lewis acid/base bonds.[6] In contrast, the latter class of hybrids have drawn much more attention than the former ones not only for they can overcome the disadvantages of the former ones of the quenching effect of luminescent centers, inhomogeneous dispersion of the two phases, leaching of the dopants, or clustering of emitters, but also because they belong to the molecular-based composite materials with excellent chemical stability and a monophasic appearance even with a high concentration of lanthanide complexes. Thus we can tailor the multifunctional advanced materials for different demands in physiology, biochemistry, and photochemistry areas through the combination of the different components with chemical bonds.

Zeolites are a class of aluminosilicates with relatively rigid anionic frameworks and crystallographically well-defined nanometer-sized channels or cavities. They can host a great variety of photochemically and photo-physically active guests. An increased chemical or thermal stability of the inserted species can often be observed in such host–guest materials. Therefore, they have attracted considerable interest for constructing novel optical materials.[7] The versatility of pore structure and morphologies provided by different types of zeolite offers many possibilities for the design of host–guest systems with specific properties.[8] Among them, zeolite A (ZA) is structurally the most simple zeolite, [9] but less attention has paid to it to construct lanthanide based host-guest systems. Therefore, it is essential to shed some light on zeolite A as the matrix of lanthanide complexes. Zeolite A has a three-dimensional network of $[AlO_4]^{5-}$ and $[SiO_4]^{4-}$ tetrahedra linked via bridging oxygen atoms with

smallest and largest free diameters of 0.41 nm and 1.14 nm, respectively. The formula of the synthetic zeolite A is $Na_{96}[(AlO_2)_{96}(SiO_2)_{96}]\cdot 216H_2O$ according to X-ray structural analysis studies where each aluminum unit introduces a negative charge that must be compensated by cationic species Na^+. These cations are ionically bound to the zeolite framework and can be readily exchanged by other cations such as Eu^{3+} and Tb^{3+}.[10] The ion-exchange property of zeolite can make lanthanide complexes encapsulated into zeolite cages through strong coordination effects between lanthanide ions and skeleton oxygen atoms, thus converting zeolite A into luminescent materials.[11] In addition, the regularly distributed silanol groups covered on the surface of zeolite A also can make zeolite to be optical materials. In general, this is achieved via a trialkoxysilyl derivative of a polydentate ligand that not only can coordinate and sensitize the lanthanide ions, but also can bind on the zeolite matrix.[12] As a result, the lanthanide complexes can covalently graft onto the external surface of zeolite A. From the above, through chemical bonding force lanthanide complexes can be introduced both inside and outside zeolite A facilely.

However, a drawback of zeolite particles is their tendency to aggregate and their pronounced light scattering in the visible range, which hampers the optical use of the host-guest materials. Therefore, it is highly interesting and desirable to make the materials transparent for fabrication of different photonic devices. Embedding zeolite into an organic polymer which possesses the properties of flexibility and transparency can lead to novel transparent lanthanide/inorganic/organic polymeric hybrid materials. The most extensive method to construct the lanthanide polymeric hybrids is that the polymer unit behaves as the ligand to coordinate to central lanthanide ions.[13] The organic polymers, such as poly(methylmethacrylate),[14] poly(vinylpyridine),[15] poly(vinylpyrrolidone),[16] poly(ethylene glycol),[17] and so on, are suitable ligands for lanthanide ions in view of their low optical absorption in the ultraviolet-visible region, favorable coordination atoms in the structure, easily processed method, and low synthetic cost. And it is proved that these kinds of materials can be expected to possess the more effective property such as stronger luminescence intensities, longer lifetimes and higher luminescence quantum efficiencies, because the introduction of organic polymer chain is beneficial to the luminescence of the whole hybrid system for it can prevent water molecules from quenching the emission of lanthanide ions.

In this study, our research aim is to construct new types of photo-functional hybrid materials based zeolite A and polymer, which can be expected to have potential application in the practical fields of optical devices for display and lighting. In a first step, the zeolite A crystals are loaded with the desired guest species-lanthanide complexes. Once this is done, the external surface of the zeolite A is modified by first functionalizing zeolite A with a muti-functional linker (TAA-Si/AA-Si) and then covalently grafting lanthanide ions which coordinates to both the molecular linker and the polymer chain. The TAA-Si or AA-Si is obtained by modifying active methylene of 1,1,1-Trifluoroacetylacetone (TAA) or acetylacetone (AA) by 3-(triethoxysilyl)propyl isocyanate (TEPIC) bearing trialkoxysilyl groups , and the as-obtained molecular linker have the ability to bind on zeolite A and to coordinate and sensitize Ln^{3+}ions. Finally, the transparent polymer thin films were made by spin-coating. Full characterizations and detailed studies of the luminescence properties of these materials were investigated and compared.

Experimental section

Chemicals. Chemically pure and highly crystalline zeolite A (ZA) was synthesized and characterized as described previously.[18] The crystals with the morphology of typical truncated cubes (rhombic dodecahedra) were used in this study. Solutions of $TbCl_3\cdot 6H_2O$ and $EuCl_3\cdot 6H_2O$ in ethanol were obtained by dissolving Tb_4O_7 and Eu_2O_3 in hydrochloric acid (37 %) followed by evaporation and solvation in ethanol, respectively. 2-Thenoyltrifluoroacetone (99 %, TTA, Adamas), 1,1,1-trifluoroacetylacetone (98 %, TAA, Adamas), 3-(triethoxysilyl)propyl isocyanate (96 %, TEPIC, J&K Scientific LTD), 4-vinylpyridine (95 %, 4VP, J&K Scientific LTD), ethyl methacrylate (99 %, EMA, Aladdin) were used as received. The super dry solvent tetrahydrofuran (THF) was directly purchased from J&K Scientific LTD and used as received. All the other reagents are analytical pure and purchased from China National Medicines Group.

Synthetic procedures.

Preparation of the cross-linking precursor containing Si-O chemical bonds (TAA-Si / AA-Si) [13(a), 19]: The whole procedure for the preparation of TAA–Si or AA-Si was under an atmosphere of argon. Typically, 4 mmol NaH (0.16 g, 60 %) was first added to a small round-bottomed flask. Then, 20 mL anhydrous tetrahydrofuran (THF) and 2 mmol 1,1,1-trifluoroacetylacetone (TAA) or acetylacetone (AA) were successively injected into the flask under stirring. Two hours later, 4 mmol (1.0 g) 3-(triethoxysilyl)propyl isocyanate (TEPIC) dissolved in 20 mL THF was put into the solution by drops for half hour. The whole mixture was refluxing at 333K for 12 hrs. The product was obtained by concentrating under room temperature to remove the solvent THF using a rotary vacuum evaporator. In controlled experimental conditions (dry organic solvent and argon atmosphere), the organosilyl-β-diketone ligand was synthesized in good yield (85 %). The ethyl-silylated ligand obtained by the α-carbon substitution from β-diketone ligands was corroborated by the ^1H and ^{13}C NMR spectra. IR: σ 1690 cm^{-1} (–CONH–), σ 2980 cm^{-1} (CH_2), σ 1101 cm^{-1} (Si-O). ^1H NMR (TAA-Si) ($CDCl_3$, 500 MHz): δ 0.68 (t, 4H, –CH_2-Si–), δ 1.22 (t, 18H, –Si-O-CH_2–), δ 1.60 (m, 4H, –CH_2–), δ 2.1 (s, 3H, –CH_3CO–), δ 3.15 (m, 4H,–CH_2–), δ 3.85 (q, 12H, –Si-O-CH_2–), δ 8.0 (t, 2H, –NH–); ^{13}C NMR ($CDCl_3$): δ 207 (C=O), δ 172 (－NH-C=O), δ 76.5 (C), δ 125.5 (CF_3), δ 51 (－OCH_2－), δ 45.5 (－NH-CH_2－), δ 19 (CH_3), δ 16.5 (CH_2), δ 8.8 (－Si-CH_2－). ^1H NMR (AA-Si) ($CDCl_3$, 500 MHz): δ 0.68 (4H, –CH_2-Si–), δ 1.22 (18H, –Si-O-CH_2–), δ 1.70 (4H, –CH_2–), δ 2.19 (6H, –CH_3CO–), δ 3.40 (4H,–CH_2–), δ 3.83 (12H, –Si-O-CH_2–), δ 8.0 (2H, –NH–); ^{13}C NMR ($CDCl_3$): δ 206 (C=O), δ 171.9 (－NH-C=O), δ 98 (C), δ 51.2 (－OCH_2－), δ 45 (－NH-CH_2－), δ 17.5 (CH_3), δ 16.5 (CH_2), δ 8.5 (－Si-CH_2－).

Preparations of Ln-ZA (Ln = Eu or Tb): The Ln-ZA samples were prepared by ion-exchange.[9(b),20] The zeolite was exchanged with Ln^{3+} ions by stirring 150 mg of zeolite powders with 1.5 mL of

ethanol $LnCl_3 \cdot xH_2O$ solution ($0.1 mol \cdot L^{-1}$) for 24 hrs. The pH of the solution was ca. 6. The exchanged zeolite was centrifuged off, washed three times with ethanol and dried at 353 K under normal atmospheric conditions.

Preparations of $Eu(TTA)_n$-ZA and $Tb(TAA)_n$-ZA: The organolanthanide-zeolite A materials were synthesized by using the ship-in-bottle method.[21] The Ln-ZA samples were degassed and dried for 2 hrs at 423 K and then kept in contact with the vapor of the ligands (TTA or TAA) at 323 K overnight. The resulting material was washed with CH_2Cl_2, in order to remove only physically adsorbed ligand, and dried at 313 K in vacuum.

Synthesis of PEMA-P4VP-Ln-TAA-Si-[$Ln(L)_n$-ZA][12(b), 13(a), 19(a)]: A stoichiometric amount of TAA–Si was dissolved in 20 mL THF with stirring and a corresponding amount of $LnCl_3 \cdot 6H_2O$ was added to the solution. The reaction mixture was agitated magnetically for 5 hrs at 313 K. And then a certain amount of 4-vinylpyridine (4VP) was added to continue to react with the above solution for another 5 hrs (the molar ratio of $LnCl_3 \cdot 6H_2O$/TAA-Si/4VP was 1 : 2 : 4). After the coordination reactions had completed among TAA-Si, $LnCl_3 \cdot 6H_2O$ and 4VP, 0.5 mL of liquid monomer ethyl methacrylate (EMA) was then introduced to the above mixture, followed by initiator benzoyl peroxide (BPO). The amount of initiator was 0.4 – 0.5 % of the monomer. The mixed solution is continued agitated magnetically for approximately 6 hrs at 353 K to obtain the polymers (PEMA-P4VP)which were constructed through addition polymerization between 4VP and EMA under argon atmosphere. After that, the 10 wt % $Ln(L)_n$-ZA powder was added and continued to reflux for 20 hrs at 353 K to make sure TAA–Si can be anchored onto $Ln(L)_n$-ZA. The obtained materials were concentrated under room temperature to remove the solvent THF using a rotary vacuum evaporator, and the resulting product was viscous liquid. PEMA-P4VP-Ln-AA-Si-[$Ln(L)_n$-ZA] is prepared in the same way as described for PEMA-P4VP-Ln-TAA-Si-[$Ln(L)_n$-ZA] except that TAA-Si is replaced by AA-Si.

Preparations of thin films [22]: The luminescent polymer thin films of zeolite A assemblies were prepared by direct spin-coating method through dropping the above colloid dissolving in proper amount of THF onto a pre-cleaned 1 cm × 1 cm ITO glass which was fixed on a Laurell spin-coater. The spin rate and spin time were kept at 1000 rpm for 60 s. The solvent adsorbed was removed by drying the thin films at room temperature after spin-coating.

Physical characterization

The crystalline phases of the products were determined by X-ray powder diffraction patterns (XRD) using a Rigaku D/max-Rb diffractometer equipped with Cu anode, employing a scanning rate of 0.1 $°s^{-1}$ in the 2θ range of 5 – 65 °. Fourier transform infrared spectra (FTIR) were recorded with a Nexus 912 AO446 infrared spectrum radiometer within the wavenumber range 4000 – $400 cm^{-1}$ using the KBr pressed technique. ^1H and ^{13}C nuclear magnetic resonance (NMR) spectra were recorded in $CDCl_3$ on a Bruker AVANCE-500 spectrometer with tetramethylsilane (TMS) as internal reference. Scanning electronic microscope (SEM) images were taken using a Hitachi S-4800 microscope. Size distribution was determined on a Zetasizer Nano ZS90 instrument. The excitation and emission spectra of the thin films were obtained on an Edinburgh Instruments FLS920 spectrofluorimeter equipped with both continuous (450W) and pulsed xenon lamps. Luminescence lifetime measurements were performed with the same spectrophotometer.

Results and discussion

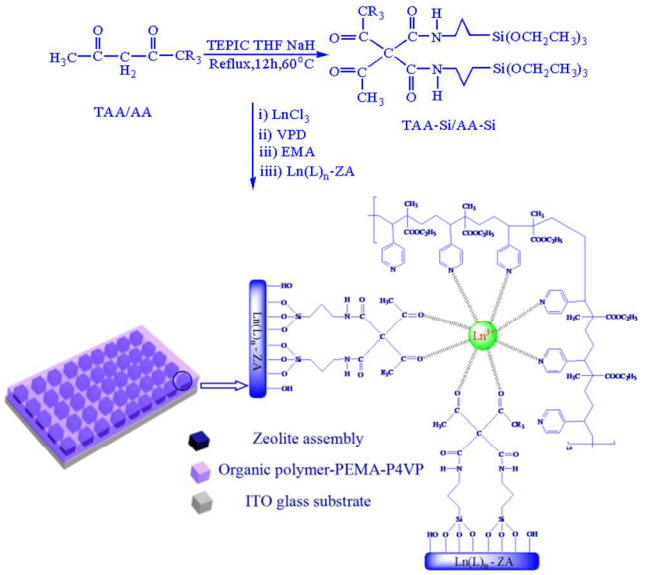

Scheme 1 Synthetic procedures and predicted structure of the polymer thin films of PEMA-P4VP-Ln-TAA-Si/AA-Si-[Ln(L)-ZA]

The as-prepared thin films using ITO glass as the substrate can be roughly denoted as the left structure in Scheme 1. The lanthanide-based zeolite A crystals whose morphology are cubic are uniformly dispersed in the organic polymer-PEMA-P4VP via the coordination effects between lanthanide ions grafted on the external surface of lanthanide loaded zeolite A and the PEMA-P4VP polymer chains. The intrinsic transparent characteristic of the organic polymer can lead to the final thin films possess a certain transparency demonstrating by the UV-vis transmittance spectra in Figure 1, in which we can see the transmittance of pure polymer (red line) and hybrid polymer (blue line) is about 90 % in the range of 400 – 700 nm and there's no transparency loss after embedding the lanthanide-zeolite assembly into the pure organic polymer.

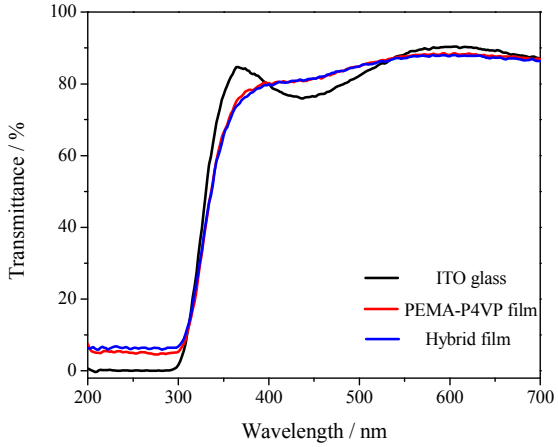

Figure 1 UV-vis transmittance spectra of ITO glass substrate (black line), pure polymer PEMA-P4VP film (red line) and the final hybrid polymer thin films (blue line).

The hybrid materials belong to a complicated system, so it is difficult to prove their exact structures. However, the main composition, the coordination effects according to the lanthanide coordination chemistry principle, and the functional groups of the organic unit can be predicted. Scheme 1 describes the predicted structure of zeolite assembly. The lanthanide ions linked outside zeolite A coordinate with the multifunctional molecule linker–TAA-Si/AA-Si and polymer chain.

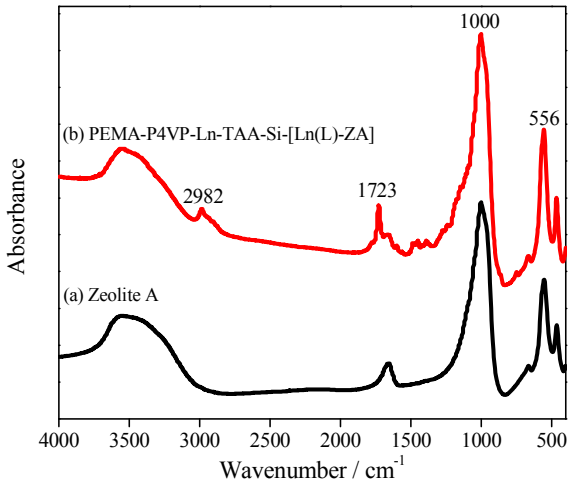

Figure 2 FT-IR spectra of (a) zeolite A and (b) PEMA-P4VP-Ln-TAA-Si-[Ln(L)$_n$-ZA].

The IR spectra of Zeolite A and the hybrid material of PEMA-P4VP-Ln-TAA-Si-[Ln(L)$_n$-ZA] are shown in Figure 2. The strongest absorption band appearing at 1000 cm^{-1} which is relative to the zeolite A host structure is assigned to the anti-symmetric stretching vibrations of T-O bonds (where T = Si or Al) in TO_4 tetrahedra. The peak at 556 nm belongs to the typical vibrations of the double four-membered rings (D4R) which are a part of the secondary building units (SBU) forming zeolite A. The T-O-T bending vibration can be observed at 460 cm^{-1}.[23] The hybrid material fabricated lanthanide complexes shows the similar infrared absorption bands as the zeolite A framework except two absorption bands at 2982 cm^{-1} and 1723 cm^{-1}, which are the absorption bands of –CH_2– and C=O groups from TAA-Si, respectively. The absence of the characteristic peaks of the trialkoxysilyl group {Si-(OCH_2CH_3)$_3$} of TAA-Si at 2977, 2922 and 2886 cm^{-1} and the only one peak at 2982 cm^{-1} indicate the trialkoxysilyl group reacts with the silanol groups covered on the surface of zeolite A, thus corroborating TAA-Si has been successfully grafted onto the external surface of lanthanide loaded zeolite A.[13(a),19(a),24]

SEM image of pure zeolite A is given in Figure 3 (a), in which we can see the shape morphology of zeolite A is the typical truncated cubes (rhombic dodecahedra). The SEM image and the size distribution histogram in Figure 3 (a) showed that the zeolite A particles were monodispersed with an average particle size of 2.0 um. Dispersion of the lanthanide loaded zeolite A in the polymer matrix through chemical bond was investigated by surface and cross-section SEM, as shown in Figure 3 (b, c, d). Several white spots in the images which are even distributed on the smooth background of the PEMA-P4VP polymer originate from zeolite A. And from the surface and cross-section images, we can further infer a homogeneous dispersion of zeolite crystals throughout a polymer matrix.

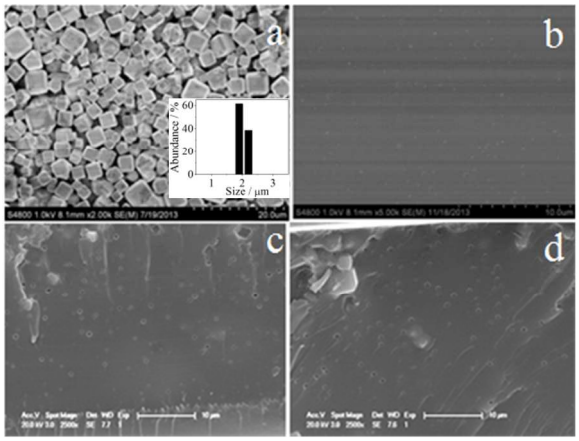

Figure 3 SEM images of (a) zeolite A and typical (b) surface and (c, d) cross-sectional SEM images of hybrid polymer thin film. The histogram of size distribution of zeolite A was shown in the bottom right of image (a).

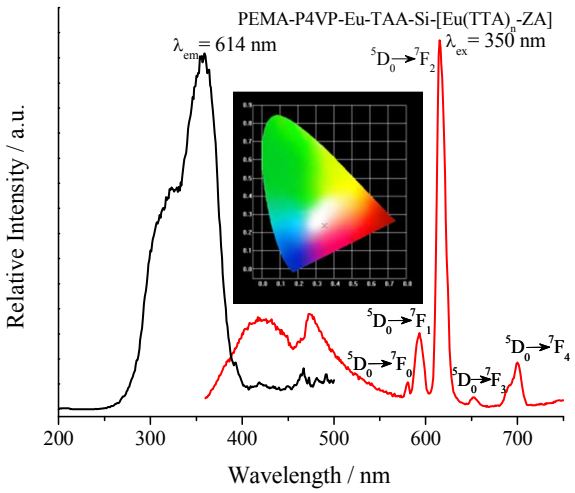

Figure 4 The excitation (black line) and emission spectra (red line) of PEMA-P4VP-Eu-TAA-Si-[Eu(TTA)$_n$-ZA] and its CIE chromaticity diagram.

In Figure 4 it is presented the excitation spectra of the PEMA-P4VP-Eu-TAA-Si-[Eu(TTA)$_n$-ZA] hybrid material registered at room temperature by monitoring the luminescence intensity of the $^5D_0 \rightarrow {}^7F_2$ transition at 614 nm. It is observed that in the spectral region from 200 to 500 nm, the material exhibits two intense broad excitation bands centered at 322 and 350 nm, which can be attributed to $\pi \rightarrow \pi^*$ electron transitions of the ligands (TAA-Si and TTA). Furthermore, the typical intra-configurational transitions of the trivalent europium ions exhibit very low intensity in the excitation spectra compared with the result of excitation spectrum in Figure S4, corroborating an efficient energy transfer from the organic ligands to the metal ions. The optical data suggest that both TTA ligands in the cages of zeolite A and TAA-Si on the surface of zeolite A are efficient sensitizers for the Eu^{3+} ions. Figure 4 also displays the emission spectra recorded under excitation at 350 nm in the spectral range of 380 to 750 nm. The emission bands were observed at 580, 592, 614, 652 and 700 nm and were attributed to f–f transitions of Eu^{3+}: $^5D_0 \rightarrow {}^7F_0$ (zero–zero band: forbidden transition), $^5D_0 \rightarrow {}^7F_1$ (magnetic dipole transition), $^5D_0 \rightarrow {}^7F_2$, $^5D_0 \rightarrow {}^7F_3$ and $^5D_0 \rightarrow {}^7F_4$

(electric dipole transitions), respectively. The presence of only one sharp peak of the non-degenerate $^5D_0 \rightarrow {}^7F_0$ transition at around 580 nm indicates that the Eu^{3+} ion occupies only a single site and a single chemical environment of symmetry C_s, C_n or C_{nv} exists around it when excited at 350 nm.[25] The peaks at around 592 nm ($^5D_0 \rightarrow {}^7F_1$) and 614 nm ($^5D_0 \rightarrow {}^7F_2$) yields the orange-red and red colors, respectively. The $^5D_0 \rightarrow {}^7F_1$ transition is allowed by a magnetic dipole transition, and it is usually taken as a standard transition, because the intensity of a magnetic dipole is largely independent of the local environment of Eu^{3+} ions. The most intense emission in the luminescent spectra is the $^5D_0 \rightarrow {}^7F_2$ transition, the so-called hypersensitive transition, at 614 nm, which is responsible for the brilliant-red emission of the hybrid material. In general, the Eu^{3+} ions can be used as a probe for the crystal field environments through comparison of the intensity of the $^5D_0 \rightarrow {}^7F_1$ (592 nm) transition with that of the $^5D_0 \rightarrow {}^7F_2$ (614 nm) transition, because the intensity ratio (R) of the $^5D_0 \rightarrow {}^7F_2$ line to that of the $^5D_0 \rightarrow {}^7F_1$ line is very sensitive to the structural change in the vicinity of Eu^{3+} ions. If Eu^{3+} is in an inversion center, the magnetic dipole transition is dominant, while in a site without inversion symmetry, the $^5D_0 \rightarrow {}^7F_2$ electronic transition becomes the strongest one. It has been generally accepted that the asymmetry parameter R becomes larger while the interaction of Eu^{3+} with its neighbors becomes stronger and the Eu^{3+} site symmetry becomes lower. The R value (4.83) of our sample indicates that the local surrounding is highly asymmetric if taking into account the fact that the R value is 0.43, reported for Eu^{3+} in aqueous solution, in which they are directly coordinated to 8–9 water molecules.[26] Therefore, the much stronger intensity of the $^5D_0 \rightarrow {}^7F_2$ transition than those of other transitions suggests that the Eu^{3+} ion is indeed in a site without a center of inversion and the material has good color purity.[27] The broad emission band in the range of 400 – 500 nm, we speculate, maybe the emissions of zeolite A and/or the polymer of PEMA-P4VP according to the luminescence behavior of zeolite A in Figure S2 and organic polymer in Figure S3. The combined emissions of host matrices in the blue region and Eu^{3+} in the red region lead to a white light, displaying in the CIE diagram in Figure 4, with the chromaticity coordinates of (0.3469, 0.2383) when excited at 350 nm.

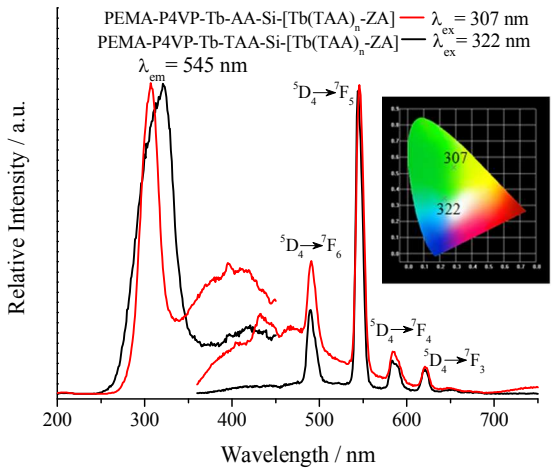

Figure 5 The excitation and emission spectra of terbium hybrids of PEMA-P4VP-Tb-AA-Si-[$Tb(TAA)_n$-ZA] (red line) and PEMA-P4VP-Tb-TAA-Si-[$Tb(TAA)_n$-ZA] (black line) and their CIE chromaticity diagram.

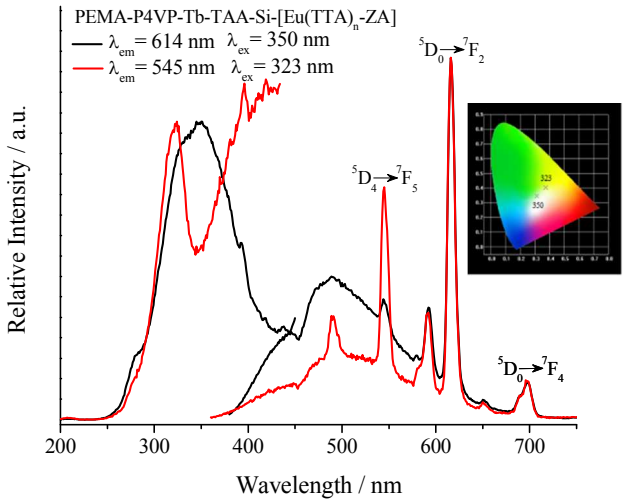

Figure 6 The excitation and emission spectra of PEMA-P4VP-Tb-TAA-Si-[$Eu(TTA)_n$-ZA] (black line: λ_{em} = 614 nm, λ_{ex} = 350 nm; red line: λ_{em} = 545 nm, λ_{ex} = 323 nm) and its CIE chromaticity diagram.

Figure 5 shows the excitation spectra of two terbium hybrids monitored by emission wavelength at 545 nm, both of which show the similar excitation character. The excitation spectrum of each material consists a main broad band centered at about 307 nm and 322 nm, respectively, which can be mainly ascribed to the transitions involving the $\pi \rightarrow \pi^*$ states of the organic units (TAA and AA-Si/TAA-Si).The strong broad excitation bands of the organic units are beneficial for the luminescence sensitization of the Tb^{3+} ions. The emission spectra obtained under the maximum excitation wavelength at 307 and 322 nm, respectively, are composed of four apparent emission lines at 490, 545, 587 and 622 nm assigned to the $^5D_4 \rightarrow {}^7F_J$ (J = 6 – 3) transitions of Tb^{3+} along with blue emissions of the host matrices in the short wavelength region of less than 500 nm. The most intense peak appearing at 545 nm which is ascribed to magnetic dipole transition results in bright-green luminescence. The absence of the ligand-based emission in the fluorescence spectra indicates that the ligand absorb and transfer energy quite efficiently to the Tb^{3+} ions. According to Dexter's theory,[28] the suitability of the energy difference between the triplet state of the ligands and the resonance level of the Ln^{3+} ions is a critical factor for efficient energy transfer, and the energy transfer is not efficient when the energy difference is too big or too small. For the ligand used in our system, energy will efficiently transfer from TTA or TAA-Si ligands to the 4f levels of the $^5D_0$ (17250 cm^{-1}) states of Eu^{3+} ions and from TAA or AA-Si ligands to the $^5D_4$ energy level (21000 cm^{-1}) of the Tb^{3+} ions. The chromaticity coordinates (x, y) of both terbium hybrid materials are also obtained and the emission of both hybrids lies in the blue-green and green region, with coordinates of (0.2308, 0.3435) for PEMA-P4VP-Tb-AA-Si-[$Tb(TAA)_n$-ZA], and of (0.2874, 0.5349) for PEMA-P4VP-Tb-TAA-Si-[$Tb(TAA)_n$-ZA] when excited at 307 and 322 nm, respectively.

Among the lanthanide ions, the Eu^{3+} and Tb^{3+} ions are two of the most important luminescent activators, which are attractive in visible luminescent materials owing to their strong red and green emissions. Besides, the polymer and zeolite A used in our system can emit blue lights. Considering the Eu^{3+}, Tb^{3+} and polymer/zeolite A exhibiting the primary colors (blue, red and green), it is expected

that we can obtain materials with tunable optical activity and white light-emitting through embedding of Eu^{3+} and Tb^{3+} ions into the polymer or zeolite A. This would be of interest because the white light-emitting compounds have extensive applications in general lighting sources. A variety of Eu^{3+} and Tb^{3+} co-doped hybrid materials were prepared, shown as PEMA-P4VP-Ln_2-TAA-Si/AA-Si-[$Ln_1(L)_n$-ZA]. The emission and excitation spectra of these types of materials measured at 298 K are listed in Figures 6 – 8.

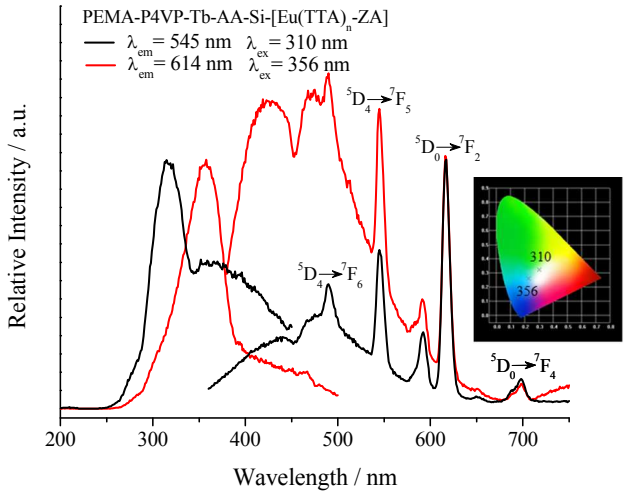

Figure 7 The excitation and emission spectra of PEMA-P4VP-Tb-AA-Si-[Eu(TTA)$_n$-ZA] (black line: λ_{em} = 545 nm, λ_{ex} = 310 nm; red line: λ_{em} = 614 nm, λ_{ex} = 356 nm) and its CIE chromaticity diagram.

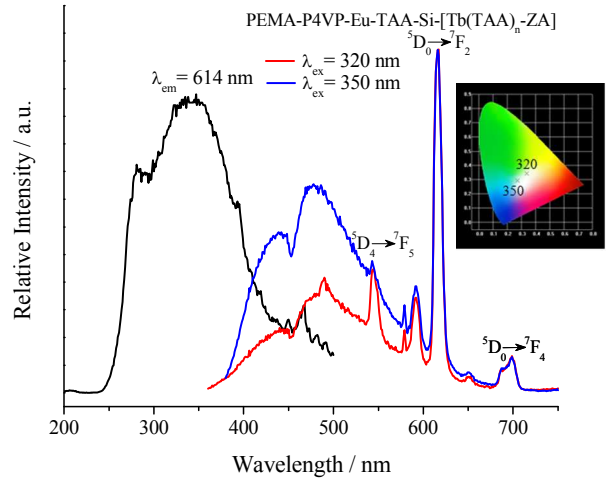

Figure 8 The excitation (black line) and emission spectra (red line: λ_{ex} = 320 nm; blue line: λ_{ex} = 350 nm) of PEMA-P4VP-Eu-TAA-Si-[Tb(TAA)$_n$-ZA] and its CIE chromaticity diagram.

In Figure 6 by monitoring at the strongest emission peaks of Eu^{3+} (614 nm) and Tb^{3+} (545 nm), respectively, obtained the broad excitation bands with different maximum wavelength which are produced by diverse ligands coexisting in the material, TTA, TAA-Si and 4VP. The excitation spectra in Figure 7 show the similar property. Excited at the maximum excitation wavelength, the Eu^{3+} and Tb^{3+} co-doped hybrid materials exhibit a broad band ranging from 400 to 500 nm and six narrow emission peaks centered at 490 nm ($^5D_4 \rightarrow {}^7F_6$), 545 nm ($^5D_4 \rightarrow {}^7F_5$), 592 nm ($^5D_4 \rightarrow {}^7F_4$ or $^5D_0 \rightarrow {}^7F_1$), 614 nm ($^5D_0 \rightarrow {}^7F_2$), 652 nm ($^5D_0 \rightarrow {}^7F_3$) and 700 nm ($^5D_0 \rightarrow {}^7F_4$) which are responsible for the characteristic blue, green, and red colored emissions of the polymer, terbium, and europium complexes, respectively. The photoluminescence of the Red-Green-Blue (RGB) materials can be tuned during the utilization by changing the excitation wavelength which has effects on the emission intensity ratio of the three colored components, as revealed by Figures 6 – 8. Along with the increase of excitation wavelength from 323 to 350 nm, 310 to 356 nm or 320 to 350 nm, we can see the luminescence intensity of the polymer becomes intense, thus causing that the point of emission spectra in CIE chromaticity diagram shifts from yellow-white (x = 0.3736 and y = 0.4023) to white (x = 0.3135 and y = 0.3441), white (x = 0.303 and y = 0.322) to blue (x = 0.2272 and y = 0.2603) and white (x = 0.3381 and y = 0.3427) to blue-white (x = 0.273 and y = 0.2934), respectively. Through tuning the excitation wavelength, the simultaneous emission bands in the red, green, and blue regions can combine to give a pure white light of all the three materials. The calculated chromaticity coordinates which fall well in the white region of CIE chromaticity diagram as displayed in Figures 6 — 8 are close to the standard equal energy white light illuminate (x = 0.333, y = 0.333), thus ideal for the white-light emission.

The typical decay curves of the europium and terbium hybrid materials were measured, and all the decay curves follow a single-exponential function ($Ln(S(t)/S_0) = -k_1t = -t/\tau$). The lifetime data of the obtained hybrid materials are given in Table 1.

Table 1 The luminescence data of the hybrid materials.

Materials	λ_{ex} (nm)	λ_{em}(nm)	τ (μs)
PEMA-P4VP-Eu-TAA-Si-[Eu(TTA)$_n$-ZA]*	350	614	517
PEMA-P4VP-Tb-AA-Si-[Tb(TAA)$_n$-ZA]	307	545	451
PEMA-P4VP-Tb-TAA-Si-[Tb(TAA)$_n$-ZA]	322	545	791
PEMA-P4VP-Tb-TAA-Si-[Eu(TTA)$_n$-ZA]	323	545	496
	350	614	550
PEMA-P4VP-Tb-AA-Si-[Eu(TTA)$_n$-ZA]	310	545	476
	356	614	526
PEMA-P4VP-Eu-TAA-Si-[Tb(TAA)$_n$-ZA]	320	614	627
	350	614	564

* the intensity ratios of $^5D_0 \rightarrow {}^7F_2$ to $^5D_0 \rightarrow {}^7F_1$ is 4.83; λ_{ex}, excitation wavelength; λ_{em}, emssion wavelength; τ, lifetime.

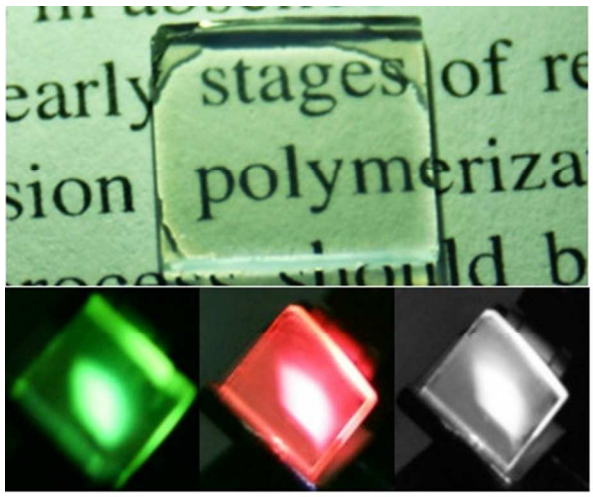

Figure 9 Photographs of the transparent thin films (top) and the photoluminescence colors from the organic polymer thin films with the UV excitation using a Xe lamp as the excitation source (bottom). The images from left to right stands for terbium hybrids, europium hybrids, and Eu^{3+}/Tb^{3+}

co-doped hybrids, respectively. The white spots are reflections from the light source.

Photographs of the thin films are as exhibited in Figure 9. The top photograph displays the transparency of the film. In this system, we can obtain three kinds of photoluminescence colors which are green light, red light, white light from europium hybrids, terbium hybrids and Eu^{3+}/Tb^{3+} co-doped hybrid materials, respectively. The white spots in the photograph are reflections from the light source.

Conclusions

In summary, the PEMA-P4VP polymer thin films co-doped with the lanthanide-zeolite A via coordination bond were prepared and characterized. This was achieved by a two-step procedure. Firstly, the lanthanide complexes were embedded into the cages of zeolite A, which leads to lanthanide-zeolite A host–guest materials with a marked enhancement of thermal stability or photo-stability as well as attractive luminescent properties. Then we chose two trialkoxysilyl derivatives of polydentate ligands as bridging molecules to graft the lanthanide complexes which coordinates to the polymer chain onto the external surface of lanthanide doped zeolite A successfully, demonstrating by FT-IR, thus dispersing lanthanide based zeolite A into the organic polymer evenly which is proved by SEM. The properties of flexibility and transparency of organic polymer can lead to novel transparent lanthanide/inorganic/organic polymeric hybrid materials, thus can make it to be further applied in optical devices. The resulting transparency organic polymer thin films maintain the characteristic luminescence of lanthanide, as shown in the photoluminescence spectra, and emit light with tunable colors depending on the use of different lanthanide ions. Furthermore, bright white light is obtained for the composition of Eu, Tb and zeolite A/polymer through tricolor (RGB) mixing, suggesting these kinds of homogeneous molecular-based hybrid polymeric materials can be expected to have potential and significant applications in optical and electronic devices in the future.

Acknowledgements

This work is supported by the National Natural Science Foundation of China (91122003, 20971100), the Program for New Century Excellent talent of University (NCET-08-0398) and the Developing Science Funds of Tongji University.

Notes and references

Department of Chemistry, Tongji University, Shanghai 200092, China.
Fax: +86-21-65982287; Tel: +86-21-65984663;
E-mail: byan@tongji.edu.cn

Electronic Supplementary Information (ESI) available: [details of any supplementary information available should be included here]. See DOI: 10.1039/b000000x/

1 (*a*) J. C. G. Bünzli*, *Chem. Rev.*, 2010, **110**, 2729; (*b*) M. Elbanowski and B. Ma□kowska, *J. Photochem. Photobiol. A. Chem.*, 1996, **99**, 85.
2 (*a*) S. Comby and J. C. G. Bünzli, *Handbook on the Physics and Chemistry of Rare Earths*, 2007, **37**, 217; (*b*) W. X. Que and X. Hu, *Appl. Phys. B*, 2007, **88**, 557; (*c*) P. Escribano, B. Julián-López, J. Planelles-Aragó, E. Cordoncillo, B. Viana and C. Sanchez, *J. Mater. Chem.*, 2008, **18**, 23; (*d*) A. Le Quang, J. Zyss, I. Ledoux, V. Truong, A. M. Jurdyc, B. Jacquier, D. Le and A. Gibaud, *Chem. Phys.*, 2005, **318**, 33.
3 (*a*) L. D. Carlos, R. A. Ferreira, V. de Zea Bermudez, B. Julian-Lopez and P. Escribano, *Chem. Soc. Rev.*, 2011, **40**, 536; (*b*) K. Binnemans, *Chem. Rev.*, 2009, **109**, 4283; (*c*) L. D. Carlos, R. A. Ferreira, V. D. Z. Bermudez and S. J. Ribeiro, *Adv. Mater.*, 2009, **21**, 509.
4 (*a*) C. Sanchez and F. Ribot, *New. J. Chem.*, 1994, **18**, 1007; (*b*) C. Sanchez, F. Ribot and B. Lebeau, *J. Mater. Chem.*, 1999, **9**, 35.
5 (*a*) L. D. Carlos, R. Sá Ferreira, J. Rainho and V. de Zea Bermudez, *Adv. Funct. Mater.*, 2002, **12**, 819; (*b*) P. P. Lima, R. A. Sá Ferreira, R. O. Freire, A. Paz, A. Filipe, L. Fu, S. Alves, L. D. Carlos and O. L. Malta, *Chemphyschem*, 2006, **7**, 735; (*c*) L. N. Sun, H. J. Zhang, L. S. Fu, F. Y. Liu, Q. G. Meng, C. Y. Peng and J. B. Yu, *Adv. Funct. Mater.*, 2005, **15**, 1041; (*d*) W. Q. Fan, J. Feng, S. Y. Song, Y. Q. Lei, G. L. Zheng and H. J. Zhang, *Chem. Eur. J.*, 2010, **16**, 1903.
6 (*a*) P. Lenaerts, A. Storms, J. Mullens, J. D'Haen, C. Görller-Walrand, K. Binnemans and K. Driesen, *Chem. Mater.*, 2005, **17**, 5194; (*b*) L. N. Sun, H. J. Zhang, C. Y. Peng, J. B. Yu, Q. G. Meng, L. S. Fu, F. Y. Liu and X. M. Guo, *J. Phys. Chem. B.,* 2006, **110**, 7249; (*c*) H. Wang, Y. Ma, H. Tian, N. Tang, W. Liu, Q. Wang and Y. Tang, *Dalton. Trans.*, 2010, **39**, 7485; (*d*) Y. J. Li and B. Yan, *J. Mater. Chem.*, 2011, **21**, 8129.
7 (*a*) M. B. Roeffaers, R. Ameloot, M. Baruah, H. Uji-i, M. Bulut, G. De Cremer, U. Müller, P. A. Jacobs, J. Hofkens and B. F. Sels, *J. Am. Chem. Soc.*, 2008, **130**, 5763; (*b*) M. Busby, C. Blum, M. Tibben, S. Fibikar, G. Calzaferri, V. Subramaniam and L. De Cola, *J. Am. Chem. Soc.*, 2008, **130**, 10970; (*c*) Y. Wada, M. Sato and Y. Tsukahara, *Angew. Chem. Int. Ed.*, 2006, **45**, 1925; (*d*) M. Busby, H. Kerschbaumer, G. Calzaferri and L. De Cola, *Adv. Mater.*, 2008, **20**, 1614.
8 W. M. M. C. Baerlocher, D. H. Olson, *Atlas of Zeolite Framework Types, 5th ed., Elsevier, Amsterdam*, 2001.
9 (*a*) D. W. Breck, *Zeolite Molecular Sieves, Wiley, New York,*, 1973, **4**; (*b*) A. M. ávan der Veen, *J. Chem. Soc. Faraday Trans.*, 1992, **88**, 133.
10 M. Alvaro, V. Fornes, S. Garcia, H. Garcia, J. C. Scaiano, *J. Phys. Chem. B.*, 1998, **102**, 8744.
11 S. V. Bel'tyukova, E. I. Tselik, A. V. Egorova and O. I. Teslyuk, *J. Appl. Spectrosc.*, 2003, **70**, 307.
12 (*a*) Y. G. Wang, H. R. Li, W. J. Zhang and B. Y. Liu, *Mater. Lett.*, 2008, **62**, 3167; (*b*) H. R. Li, W. J. Cheng, Y. Wang, B. Y. Liu, W. J. Zhang and H. J. Zhang, *Chem. Eur. J.*, 2010, **16**, 2125.
13 (*a*) X. F. Qiao and B. Yan, *Inorg. Chem.*, 2009, **48**, 4714; (*b*) B. Yan and X. F. Qiao, *J. Phys. Chem. B*, 2007, **111**, 12362; (*c*) B. Yan, Q. Kai and X. L. Wang, *Inorg. Chim. Acta.*, 2011, **376**, 302; (*d*) X. F. Qiao, H. Y. Zhang and B. Yan, *Dalton. Trans.*, 2010, **39**, 8882; (*e*) L. Guo, B. Yan, J. L. Liu, K. Sheng and X. L. Wang, *Dalton. Trans.*, 2011, **40**, 632.
14 (*a*) H. F. Jiu, J. J. Ding, Y. Y. Sun, J. Bao, C. Gao and Q. J. Zhang, *J. Non-Cryst. Solids.*, 2006, **352**, 197; (*b*) J. J. Ding, H. F. Jiu, J. Bao, J. C. Lu, W. R. Gui, Q. J. Zhang and C. Gao, *J. Comb. Chem.*, 2005, **7**, 69.
15 X. F. Qiao and B. Yan, *J. Phys. Chem. B.*, 2008, **112**, 14742.
16 (*a*) K. M. Kim, K. Adachi and Y. Chujo, *Polymer*, 2002, **43**, 1171; (*b*) X. X. Han, R. X. Zhou, X. M. Zheng and H. Jiang, *J. Mol. Catal. A: Chem.*, 2003, **193**, 103.
17 X. H. Chuai, H. J. Zhang, F. S. Li, S. B. Wang and G. Z. Zhou, *Mater. Lett.*, 2000, **46**, 244.
18 P. Lainé, R. Seifert, R. Giovanoli and G. Calzaferri, *New. J. Chem.*, 1997,**21**, 453.
19 (*a*) B. Yan, Y. Li and B. Zhou, *Microporous. Mesoporous. Mater.*, 2009, **120**, 317; (*b*) X. F. Qiao and B. Yan, *J. Phys. Chem. B*, 2009, **113**, 11865.
20 A. M. ávan der Veen, *J. Chem. Soc. Faraday Trans.*, 1992, **88**, 141.
21 Z. Guo, Y. G. Wang, H. R. Li, *J. Rare. Earths.,*2007, **25**, 283.
22 (*a*)B. Bräuer, D. R. T. Zahn, T. Rüffer and G. Salvan, *Chem. Phys. Lett.*, 2006, **432**, 226; (*b*) D. W. Schubert and T. Dunkel, *Mater. Res. Innovations.*, 2003, **7**, 314.
23 (*a*) N. Shigemoto, S. Sugiyama, H. Hayashi and K. Miyaura, *J. Mater. Sci.*, 1995, **30**, 5777; (*b*) R. R. Xu, W. Q. Pang, J. H. Yu, Q. S. Huo and J. S. Chen, *Chemistry-Zeolites and Porous Materials*, 2004.
24 H. R. Li, Y. X. Ding, P. P. Cao, H. H. Liu and Y. X. Zheng, *J. Mater. Chem.,* 2012, **22**, 4056.
25 (*a*) K. Binnemans, P. Lenaerts, K. Driesen and C. Görller-Walrand, *J. Mater. Chem.*, 2004, **14**, 191; (*b*) H. F. Brito, O. L. Malta, L. R. Souza, J. F. S. Menezes and C. A. A. Carvalho, *J. Non-Cryst. Solids*, 1999, **247**, 129.
26 (*a*) B. Julián, R. Corberán, E. Cordoncillo, P. Escribano, B. Viana and C. Sanchez, *J. Mater. Chem.*, 2004, **14**, 3337; (*b*) H. R. Li, W. J. Cheng, Y. Wang, B. Y. Liu, W. J. Zhang and H. J. Zhang, *Chem. Eur. J.*, 2010, **16**, 2125; (*c*) K. Lunstroot, K. Driesen, P. Nockemann, C. Görller-Walrand, K.Binnemans, S. Bellayer, J. L. Bideau and A. Vioux, *Chem. Mater.*, 2006, **18**, 5711.
27 H. F. Brito, O. L. Malta and J. F. S. Menezes, *J. Alloys. Comp.*, 2000, **303**, 336.
28 D. L. Dexter, *J. Chem. Phys.*, 1953, **21**, 836.

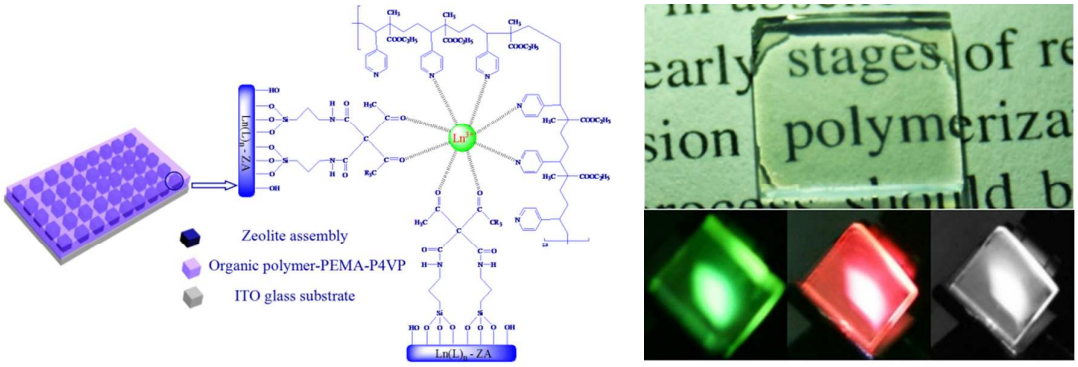

Three tricolor luminous materials based on novel transparent hybrid films of polymer-lanthanide-zeolite A were assembled. The white light-emitting from the tricolor luminous materials can be tuned easily by adjusting the different concentration of the doped ions and the excitation wavelength.